

The optical spectra of X-shaped radio galaxies

Hermine Landt^{1*}, Chi C. Cheung^{2,3} and Stephen E. Healey⁴

¹*School of Physics, University of Melbourne, Parkville, VIC 3010, Australia*

²*NASA Goddard Space Flight Center, Code 661, Greenbelt, MD 20771, USA*

³*Space Science Division, Naval Research Laboratory, Washington, DC 20375, USA*

⁴*Department of Physics, Stanford University, Stanford, CA 94305, USA*

Accepted . Received ; in original form

ABSTRACT

X-shaped radio galaxies are defined by their peculiar large-scale radio morphology. In addition to the classical double-lobed structure they have a pair of low-luminosity wings that straddles the nucleus at almost right angles to the active lobes, thus giving the impression of an 'X'. In this paper we study for the first time the optical spectral properties of this object class using a large sample (~ 50 sources). We find that the X-shaped radio population is composed roughly equally of sources with weak and strong emission line spectra, which makes them, in combination with the well-known fact that they preferentially have radio powers intermediate between those of Fanaroff-Riley type I (FR I) and type II (FR II) radio galaxies, the archetypal transition population. We do not find evidence in support of the proposition that the X-shape is the result of a recent merger: X-shaped radio sources do not have unusually broad emission lines, their nuclear environments are in general not dusty, and their host galaxies do not show signs of enhanced star formation. Instead, we observe that the nuclear regions of X-shaped radio sources have relatively high temperatures. This finding favours models, which propose that the X-shape is the result of an overpressured environment.

Key words: galaxies: active – galaxies: nuclei – galaxies: emission lines

1 INTRODUCTION

X-shaped radio galaxies are distinguished from the classical double-lobed radio sources by their peculiar large-scale radio morphology (Leahy & Parma 1992). In addition to the primary, active lobes, defined as such by having an overall higher surface brightness, they have a secondary pair of wings. These wings are located on each side of the nucleus and at large angles relative to the primary lobes, thus giving the impression of an 'X'. A prime example of this object class is the source 3C 403 (Black et al. 1992, see their Fig. 13).

Whereas agreement exists about the fact that only the pair of lobes are actively fed by radio plasma, it is not clear how the wings formed. The current propositions fall roughly into two main schools of thought: the wings are either (i) relic emission from previously active lobes or (ii) backflow emission from the primary, now active lobes. The first possibility requires a change in the jet direction, which occurred either slowly over time as jet precession (Ekers et al. 1978) or suddenly due to a flip of the black hole spin after a galaxy merger (e.g., Dennett-Thorpe et al. 2002; Merritt & Ekers

2002; Gopal-Krishna et al. 2003). The second possibility requires the presence of steep pressure gradients in the environment through which the jet propagates. These gradients are either due to an asymmetric distribution of the intracluster medium (Worrall et al. 1995) or to the shape of the host galaxy relative to the jet direction (Capetti et al. 2002). A combination of the two possibilities was proposed early on by Leahy & Williams (1984); radio plasma from the hotspots flows back preferentially into the cavities produced by the radio lobes of a previously active phase.

Observational evidence has been gathered so far mainly from studies of the radio spectral index and polarization along the lobes and wings, and from comparisons between the radio structure and the X-ray and optical morphologies of the host galaxy and immediate environment. The radio spectral index is often found to be steeper in the wings than in the lobes, indicating that the former contain older radio emission than the latter (e.g., Murgia et al. 2001; Rottmann 2001; Dennett-Thorpe et al. 2002; Lal & Rao 2007). But this result is expected in both scenarios, if the wings and lobes are relic and active emission, respectively, and if the plasma in the wings has flown first through the lobes. The direction of polarization, on the other hand, seems to favour

* E-mail: hlandt@unimelb.edu.au

the backflow scenario, since a smooth plasma stream from the active lobe to its nearest wing is almost always present.

Optical imaging revealed that X-shaped radio sources are mostly harboured by unperturbed, highly elliptical galaxies and generally live in poor clusters (e.g., Ulrich & Roenback 1996; Capetti et al. 2002; Dennett-Thorpe et al. 2002). This finding seems to disfavour a scenario, in which a recent merger has changed the jet direction. In addition, it is always found that the direction of the active lobes coincides with the *major* axis of the host galaxy, indicating that environmental effects strongly influence the resultant radio morphology of the backflow (Capetti et al. 2002; Saripalli & Subrahmanyan 2009). So far, few X-shaped radio sources have been imaged at X-ray frequencies, but all such studies favoured the backflow scenario based on the asymmetries detected in the environment (Worrall et al. 1995; Kraft et al. 2005; Miller & Brandt 2009; Hodges-Kluck et al. 2010).

In this paper we present the first systematic analysis of the optical spectra of X-shaped radio galaxies. To this end we have used a large sample, which was selected as described in Section 2, and for which we have measured selected spectral quantities as explained in Section 3. With these in hand we have addressed the issue of jet orientation and general spectral class (Section 4), we have investigated their broad and narrow emission line regions (Section 5) and we have studied the properties of the host galaxy (Section 6). Our main results are summarized in Section 7, where we also present our conclusions.

Throughout this paper we have assumed cosmological parameters $H_0 = 70 \text{ km s}^{-1} \text{ Mpc}^{-1}$, $\Omega_M = 0.3$, and $\Omega_\Lambda = 0.7$.

2 THE SAMPLE

Cheung (2007) selected from the images of the NRAO Very Large Array (VLA) FIRST survey (Becker et al. 1995) a sample of ~ 100 sources with clear or tentative X-shaped extended radio morphology. Later, Cheung et al. (2009) slightly extended this sample and defined a subsample of 50 radio galaxies with bona-fide X-shaped radio morphology and available optical spectroscopy (see their Table 2). We have considered here this radio galaxy sample to which we added two sources, namely, J1430+5217, which was identified as a quasar by the Sloan Digital Sky Survey (SDSS; Abazajian et al. 2009) but has only narrow emission lines in its spectrum (see Fig. A1), and J0245+1047, whose X-shaped radio morphology has recently been discovered by Landt & Bignall (2008). We have also included all X-shaped radio quasars with optical spectroscopy available to us (7 sources).

Cheung et al. (2009) obtained high-quality optical spectroscopy for 27/59 X-shaped radio sources and a further 19/59 sources were spectroscopically observed by the SDSS (Data Release 5; see Fig. A1). For another seven sources, namely, J0113+0106, J0115-0000, J0245+1047, J1309-0012, J1606+0000, J1952+0230, and J2347+0852, the published optical spectra were made available to us by the authors (Perlman et al. 1998; Best et al. 1999; Tadhunter et al. 1993; Lacy 2000). Table 1 lists the total spectroscopic sample used in this paper (53 sources).

The six sources excluded are J0009+1244, J0058+2651, J1424+2637, J1513+2607, J1824+7420, and J2123+2504.

3 THE SPECTRAL MEASUREMENTS

We have measured all spectral quantities on rest-frame spectra, which were corrected for Galactic extinction using A_V values derived from the Galactic hydrogen column densities of Dickey & Lockman (1990). We have measured the flux and rest-frame equivalent width by integrating the emission in the line over a local continuum using the IRAF task *onedspec.splot* and its option 'e'. In the case of blends (such as, e.g., H γ and [O III] λ 4363) we assumed Gaussian profiles and used the option 'd' of this task to deblend the individual features. However, this procedure was not necessary in the case of the SDSS spectra, whose spectral resolution ($R \sim 2000$) is sufficient to resolve all investigated lines.

We have derived 2σ upper limits on the rest-frame equivalent widths and line fluxes of the narrow emission lines [O II] λ 3727 and [O III] λ 5007 when the lines were not detected but the line position was covered by the spectrum. The non-detection limits have been calculated assuming a rectangular emission line of width 1000 km s^{-1} .

We have measured the value of the Ca II break (located at $\sim 4000 \text{ \AA}$) in spectra f_λ versus λ . The Ca II break value is defined as $C = 1 - (f_-/f_+)$, where f_- and f_+ are the fluxes in the wavelength regions $3750 - 3950 \text{ \AA}$ and $4050 - 4250 \text{ \AA}$, respectively. The Ca II break value is a suitable orientation indicator for radio-loud active galactic nuclei (AGN): the smaller its value, the smaller the jet viewing angle, i.e., the angle between the radio jet and the observer's line of sight (e.g., Landt et al. 2002).

4 ORIENTATION AND CLASSIFICATION

Landt et al. (2004) proposed a physical classification scheme for radio-loud AGN that takes into account the effects of orientation. This scheme requires the measurement of only two quantities, namely, the rest-frame equivalent widths of the narrow emission lines [O II] λ 3727 and [O III] λ 5007. Based on a bimodality observed for [O III], it then separates sources at *all* viewing angles into weak-lined and strong-lined radio-loud AGN.

In Fig. 1 we show the [O II]-[O III] equivalent width plane for the X-shaped radio sources in our spectroscopic sample, superposed with the line dividing the weak-lined and strong-lined classes (solid line) as well as the loci of constant viewing angles as obtained by Landt et al. (2004) from their simulations (dotted lines). Our optical spectra cover the locations of both [O II] and [O III] for all but one source (J0702+5002) and we list the measurements in Table 1 (columns (6) and (8)). Two important results become evident from Fig. 1. Firstly, most X-shaped radio sources are viewed at relatively large angles ($\phi \gtrsim 35^\circ$). This result is supported by their large Ca II break values. We measure $C \geq 0.25$ for all but six sources and $C \geq 0.4$ for roughly half the sample (22/53 sources; see Table 1, column (4)). The observed result is intuitive given that projection effects are expected to distort the X-shape of the diffuse radio emission at small viewing angles, thus making it difficult to recognize.

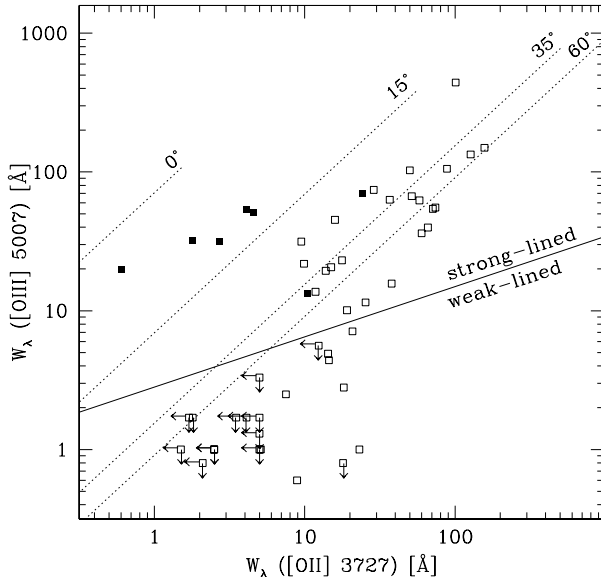


Figure 1. The rest-frame equivalent widths of [O III] $\lambda 5007$ versus [O II] $\lambda 3727$. Filled and open squares indicate sources with and without broad emission lines, respectively. Arrows indicate upper limits. The solid line separates weak-lined (below the line) and strong-lined radio-loud AGN (above the line). Dotted lines represent loci of constant viewing angles as labelled.

However, it also means that strongly relativistically beamed X-shaped radio galaxies (i.e., X-shaped radio quasars) will be difficult to select based on radio maps.

Secondly, roughly half the sample (23/53 sources) is classified as weak-lined radio-loud AGN (Table 1, column (5)), with about half of these objects (11/23 sources) having no [O II] or [O III] emission lines. This result is rather surprising. Since X-shaped radio sources are generally known to have their active pair of lobes terminating in pronounced hot spots, as observed for FR II radio galaxies, one would expect that, like these, they predominantly have strong optical emission lines. Are then X-shaped radio sources equally related to FR Is, which are known to have optical spectra with no or only weak emission lines, or do they simply contain an exceptionally large number of the otherwise rather rare weak-lined FR IIs (e.g., Laing et al. 1994; Tadhunter et al. 1998)?

In order to answer this question we have plotted in Fig. 2 the total radio luminosity at 1.4 GHz versus the absolute R magnitude for the strong-lined (filled symbols) and weak-lined X-shaped radio galaxies (open symbols), which we subdivided based on the presence or lack of pronounced hotspots in their active lobes into sources with FR II (squares) and ambiguous (triangles) radio morphology, respectively. Luminosities were predominantly taken from Cheung et al. (2009) and the radio morphology judged visually from the FIRST maps and, where available, also from published, deeper radio maps (see references in Cheung 2007). We have included only sources viewed at relatively large angles, i.e., without broad emission lines and with Ca II break values $C \geq 0.25$ (46 sources), since in their case relativistic beaming effects are expected to be negligible. Then, Fig. 2 represents the so-called Ledlow-Owen plot

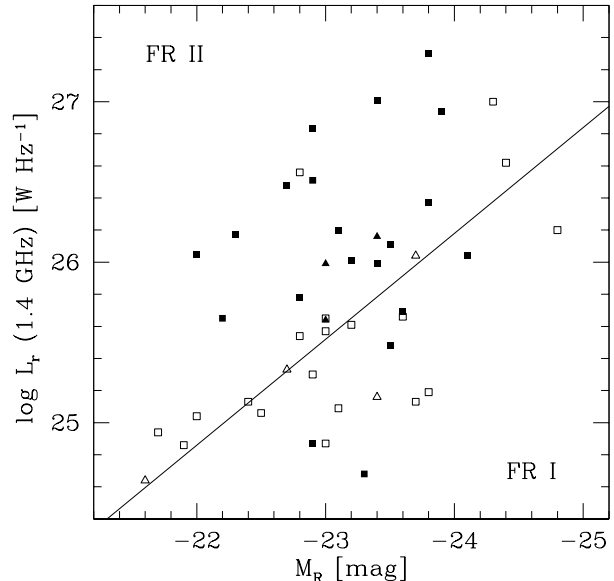


Figure 2. The radio luminosity at 1.4 GHz versus absolute R magnitude for X-shaped radio galaxies. Filled and open symbols indicate sources classified as strong-lined and weak-lined radio-loud AGN, respectively. Squares and triangles indicate sources with an FR II and ambiguous radio morphology of the active lobes, respectively. The solid line represents the division between FR I (below the line) and FR II radio galaxies (above the line) derived by Ledlow & Owen (1996), scaled to the units of the figure as in Cheung et al. (2009).

(Ledlow & Owen 1996), i.e., extended radio emission versus host galaxy luminosity, in which FR I and FR II galaxies separate (below and above the solid line, respectively). This separation, however, does not occur suddenly but rather via a transition region (Best 2009).

Fig. 2 shows that the large majority of weak-lined sources straddle the FR I/II dividing line, as X-shaped radio galaxies generally do (Leahy & Parma 1992; Dennett-Thorpe et al. 2002; Cheung et al. 2009), with only two (J0148+5332 and J1434+5906) and five objects (J0001-0033, J0702+5002, J0813+4347, J1005+1154, and J1614+2817) clearly in the FR II and FR I regime, respectively. All but one of these sources have active lobes with an FR II radio morphology, whereas J0813+4347 could be part of the recently identified X-shaped radio population without pronounced hotspots and similar to FR Is (Saripalli & Subrahmanyan 2009).

It seems then that X-shaped radio galaxies genuinely represent a transition population, and this in both radio power and emission line strengths. This transition is illustrated in detail in Fig. 3, where we have plotted the total radio luminosity at 1.4 GHz versus the luminosity of the narrow emission line region L_{NLR} , the latter calculated from the luminosities of [O II] $\lambda 3727$ and [O III] $\lambda 5007$ following Rawlings & Saunders (1991). As Fig. 3 shows, a clear transition point between the two classes can be identified at values of $L_{\text{NLR}} \sim 10^{35}$ W and $L_{\text{r}} \sim 10^{25.6}$ W Hz $^{-1}$ (dashed lines). Interestingly, this point lies on the strong ($P = 98.6\%$) linear correlation present for the strong-lined X-shaped radio sources (solid line).

Table 1. General Properties of the Spectroscopic Sample

Object Name	Observatory	z	C	class	[O II] $\lambda 3727$		[O III] $\lambda 5007$		Other Name
					W_λ [Å]	flux [erg/s/cm ²]	W_λ [Å]	flux [erg/s/cm ²]	
(1)	(2)	(3)	(4)	(5)	(6)	(7)	(8)	(9)	(10)
J0001–0033	SDSS 2.5 m	0.247	0.43	WL	<2.5	<6.68E–17	<1.0	<7.51E–17	
J0049+0059	SDSS 2.5 m	0.304	0.46	WL	18.0	2.35E–16	<0.8	<4.23E–17	
J0113+0106	Shane 3 m	0.281	0.31	SL	101.0	2.22E–15	441.7	1.95E–14	
J0115–0000	Shane 3 m	0.381	0.30	SL	157.0	5.96E–16	149.3	1.16E–15	4C –00.07
J0144–0830	MMT 6.5 m	0.181	0.39	WL	<1.5	<4.14E–17	<1.0	<6.49E–17	
J0148+5332	MMT 6.5 m	0.290	0.25	WL	<5.0	<2.28E–16	<1.7	<1.54E–16	3C 52
J0220–0156	MMT 6.5 m	0.173	0.35	SL	66.0	4.03E–15	39.8	6.64E–15	3C 63
J0245+1047	MMT 4.5 m	0.070	0.26	SL	15.0	5.30E–15	20.6	2.05E–14	4C +10.08
J0516+2458	MMT 6.5 m	0.063	0.33	SL	37.9	3.55E–15	15.7	4.41E–15	3C 136.1
J0702+5002	HJST 2.7 m	0.094	?	WL	?	?	5.0	8.80E–16	
J0805+2409	SDSS 2.5 m	0.060	0.47	SL	74.1	1.22E–14	55.4	2.40E–14	3C 192
J0813+4347	SDSS 2.5 m	0.128	0.45	WL	<2.1	<1.65E–16	<0.8	<1.61E–16	
J0831+3219	SDSS 2.5 m	0.051	0.44	WL	7.5	1.34E–15	2.5	1.38E–15	4C +32.25
J0845+4031	HET 9.2 m	0.429	0.31	SL	9.9	5.25E–16	21.8	2.23E–15	
J0859–0433	MMT 6.5 m	0.356	0.43	SL	19.1	3.41E–16	10.1	4.59E–16	
J0917+0523	HET 9.2 m	0.591	0.40	SL	13.8	6.26E–16	19.4	2.01E–15	4C +05.39
J0924+4233	SDSS 2.5 m	0.227	0.42	WL	<4.1	<1.25E–16	<1.7	<1.48E–16	
J0941–0143	MMT 6.5 m	0.384	0.45	WL	18.2	3.16E–16	2.8	1.20E–16	4C –01.19
J0941+3944	SDSS 2.5 m	0.108	0.38	SL	15.9	1.48E–15	45.2	1.16E–14	3C 223.1
J1005+1154	SDSS 2.5 m	0.166	0.48	WL	<2.5	<1.60E–16	<1.0	<1.99E–16	
J1015+5944	SDSS 2.5 m	0.527	0	SL	1.8	1.86E–16	32.3	2.01E–15	
J1018+2914	MMT 6.5 m	0.389	0.27	SL	51.5	3.93E–16	67.0	9.87E–16	
J1020+4831	SDSS 2.5 m	0.052	0.44	WL	23.1	2.39E–15	1.0	3.18E–16	4C +48.29
J1101+1640	MMT 6.5 m	0.071	0.45	WL	14.5	1.84E–15	4.4	1.44E–15	Abell 1145
J1130+0058	SDSS 2.5 m	0.133	0.26	SL	24.2	2.59E–15	69.9	1.51E–14	4C +01.30
J1135–0737	MMT 6.5 m	0.602	0.36	WL	20.8	1.35E–16	7.1	1.14E–16	
J1140+1057	SDSS 2.5 m	0.081	0.41	WL	5.1	5.72E–16	1.0	3.31E–16	
J1206+3812	SDSS 2.5 m	0.838	0	SL	2.7	2.55E–16	31.5*	2.18E–15*	
J1207+3352	SDSS 2.5 m	0.079	0.28	SL	36.8	5.22E–15	63.1	1.85E–14	
J1210–0341	MMT 6.5 m	0.178	0.40	WL	<3.5	<1.12E–16	<1.7	<1.38E–16	
J1218+1955	MMT 6.5 m	0.424	0.33	SL	50.0	2.87E–16	102.8	1.25E–15	4C +20.28
J1228+2642	HET 9.2 m	0.201	0.47	WL	<5.0	<4.78E–16	<1.3	<3.80E–16	
J1253+3435	MMT 6.5 m	0.358	0.30	SL	9.5	1.04E–16	31.5	6.89E–16	
J1309–0012	ESO 3.6 m	0.419	0.24	SL	58.0	1.34E–15	62.4	1.89E–15	4C +00.46
J1310+5458	HET 9.2 m	0.356	0.27	SL	71.2	1.14E–15	54.2	2.17E–15	
J1327–0203	SDSS 2.5 m	0.183	0.48	WL	8.9	3.49E–16	0.6	7.99E–17	4C –01.29
J1342+2547	HET 9.2 m	0.585	0.08	SL	10.5	1.95E–16	13.4	3.03E–16	
J1348+4411	MMT 6.5 m	0.267	0.28	WL	<12.4	<1.61E–16	<5.6	<1.43E–16	
J1357+4807	HET 9.2 m	0.383	0.26	SL	88.3	1.27E–15	105.5	3.00E–15	
J1406–0154	HET 9.2 m	0.641	0.40	SL	11.8	6.03E–17	13.7	1.71E–16	4C –01.31
J1406+0657	HET 9.2 m	0.550	0	SL	0.6	3.36E–16	19.7†	6.89E–15	
J1430+5217	SDSS 2.5 m	0.367	0.28	SL	127.0	2.02E–15	133.8	3.65E–15	
J1434+5906	HET 9.2 m	0.538	0.45	WL	14.3	7.04E–17	4.9	5.01E–17	
J1444+4147	SDSS 2.5 m	0.188	0.44	WL	1.8	7.64E–17	<1.7	<2.02E–16	
J1456+2542	HET 9.2 m	0.536	0.39	WL	<1.7	<2.19E–17	<1.7	<5.18E–17	
J1600+2058	MMT 6.5 m	0.174	0.37	SL	25.4	1.08E–15	11.5	1.25E–15	
J1606+0000	ESO 3.6 m	0.059	0.41	WL	<5.0	<1.18E–15	<1.0	<6.59E–16	4C +00.58
J1606+4517	HET 9.2 m	0.556	0.37	SL	59.9	5.15E–16	36.2	6.72E–16	
J1614+2817	MMT 6.5 m	0.108	0.42	WL	<5.0	<2.25E–16	<3.3	<3.63E–16	
J1625+2705	SDSS 2.5 m	0.526	0	SL	4.1	3.97E–16	53.9	3.01E–15	
J1952+0230	ESO 2.2 m	0.059	0.40	SL	28.8	1.36E–14	74.3	8.56E–14	3C 403
J2157+0037	SDSS 2.5 m	0.391	0.35	SL	17.7	2.56E–16	23.1	7.47E–16	
J2347+0852	KPNO 2.1 m	0.292	0	SL	4.6	2.20E–15	51.1	2.37E–14	

The columns are: (1) object name; (2) observatory at which the spectrum was obtained; (3) redshift; (4) Ca II break value (measured in spectra f_λ versus λ); (5) classification following Landt et al. (2004), where WL: weak-lined radio-loud AGN, SL: strong-lined radio-loud AGN; (6) rest-frame equivalent width and (7) flux of [O II] $\lambda 3727$; (8) rest-frame equivalent width and (9) flux of [O III] $\lambda 5007$; and (10) common object name.

* derived from [O III] $\lambda 4959$; † rest-frame equivalent width relative to general continuum

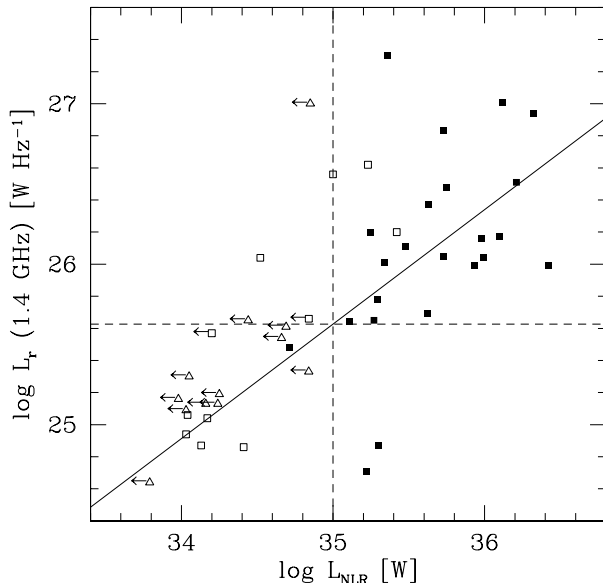


Figure 3. The radio luminosity at 1.4 GHz versus the luminosity of the narrow emission line region for X-shaped radio sources viewed at relatively large angles. Symbols are as in Fig. 2. Arrows indicate upper limits. The solid line indicates the observed correlation for the strong-lined X-shaped radio sources. The dashed lines mark the transition point in type of emission line spectrum.

Table 2. Broad Emission Line Widths

Object Name	H α λ 6563 FWHM [km/s]	H β λ 4861 FWHM [km/s]	Mg II λ 2798 FWHM [km/s]
(1)	(2)	(3)	(4)
J1015+5944	?	5727	3656
J1130+0058	7241	–	?
J1206+3812	?	8048	7473
J1342+2547	?	–	9864
J1406+0657	?	12053	8792
J1625+2705	?	7079	4074
J2347+0852	8420	7926	?

5 THE EMISSION LINE REGIONS

Seven sources in our spectroscopic sample have broad emission lines and we discuss their properties below (Section 5.1). For these (with the exception of J1406+0657) and a further 22 sources we detect besides [O II] λ 3727 and [O III] λ 5007 also other useful narrow emission lines, which we analyze in Section 5.2. We do not further discuss four sources (J1018+2914, J1253+3435, J1309–0012, and J1406–0154) that have only H β λ 4861, [O II] and [O III]. The remaining 20 sources in our sample have either no emission lines or none besides [O II] and [O III].

5.1 The Broad Emission Lines

Many popular explanations for the genesis of X-shaped radio sources require a galaxy merger, which is expected to yield a binary supermassive black hole. Such a binary can have two broad-line systems and/or two narrow-line systems, if

both supermassive black holes are quasars and their spatial separation is large enough (e.g., Peterson et al. 1987; Gaskell 1996; Boroson & Lauer 2009; Shen & Loeb 2009). In particular the two broad-line systems are expected to be observable as a single but unusually broad emission line.

In order to assess if X-shaped radio quasars have unusually broad emission lines, we have measured the full width at half-maximum (FWHM) of the most prominent lines present in our spectra, namely, the Balmer lines H α λ 6563 and H β λ 4861, and Mg II λ 2798. The narrow emission line components of H α and H β are pronounced in all objects and were removed prior to measuring the broad component. Such a correction was not straightforward for Mg II and we left the line unchanged. In Table 2 we list the measurements, where a question mark indicates that the position of the line was not covered by the spectrum. For J1130+0058 we observe broad H α , but only narrow H β . The lack of a broad H β component in this source is most likely due to dust obscuration (see Section 5.2 and Wang et al. (2003); Zhang et al. (2007)). For J1342+2547 a broad H β line appears to be present, but the spectrum is too noisy to reliably measure its width.

The observed broad emission line widths of X-shaped radio quasars span a range similar to that generally found for lobe-dominated radio quasars (Brotherton 1996; Corbin 1997; Aars et al. 2005). In this respect we note that the relatively large H β width of J1406+0657 could be due to a strong “red shelf”, an emission feature known to be associated with broad H β in some quasars (e.g., De Robertis 1985; Marziani et al. 1996). This result argues against merger models, in which the two black holes are still separated. However, it does not exclude any binary model, if it is assumed that one of the black holes has no emission line system.

5.2 The Narrow Emission Lines

The narrow emission lines probe the nuclear gas environment on scales up to a few kpc and can reveal important information that might constrain models for the origin of the X-shaped radio morphology. For example, a perturbed and rather dusty environment is expected in the case of a recent galaxy merger. On the other hand, the large pressure gradients required by the backflow model could have also increased the gas densities and/or temperatures.

In the following we estimate the nuclear dust extinction using the three strongest hydrogen lines (Section 5.2.1) and derive gas electron densities and temperatures based on sulphur and oxygen emission line ratios, respectively (Section 5.2.2). Table 3 lists the relevant flux measurements (28/53 sources).

5.2.1 Dust Extinction

We detect all three Balmer emission lines H α , H β and H γ in 11/28 sources. These sources are all but one (J0702+5002) classified as strong-lined radio-loud AGN. In Fig. 4 we compare their measured line fluxes with the predictions from Case B recombination without dust (lower solid line), and including a dust extinction of $A_V = 1$ and 2 mag (middle and upper solid lines, respectively). The values expected from Case B recombination were calculated us-

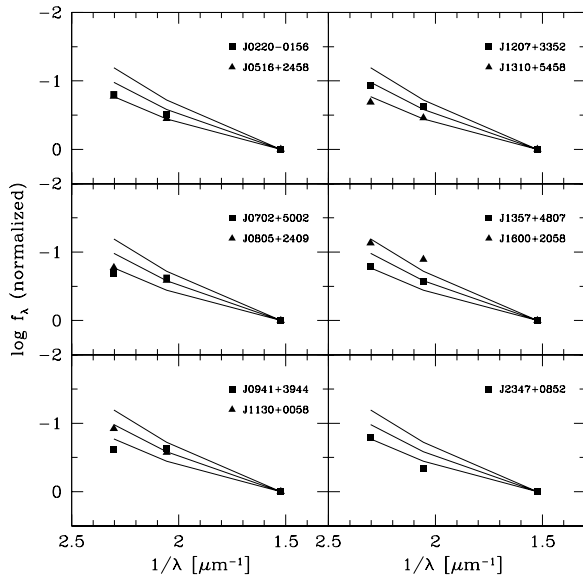


Figure 4. Balmer emission line fluxes compared to expectations from Case B recombination (for a temperature of $T = 15,000$ K and an electron density of $n_e = 10^4 \text{ cm}^{-3}$). From bottom to top, the dust extinction assumed was $A_V = 0, 1$, and 2 mag. The measurement points and the Case B solid lines were normalized to the flux of $H\alpha$.

ing the Cloudy photoionization simulation code (last described by Ferland et al. 1998) and assuming a temperature of $T = 15,000$ K and an electron density of $n_e = 10^4 \text{ cm}^{-3}$. The A_V values were transformed into A_λ values using the analytical expression for the interstellar extinction curve of Cardelli et al. (1989) and assuming a parameter $R_V = 3.1$. Fig. 4 shows the emission line fluxes and the Case B lines normalized such that the $H\alpha$ flux is unity.

In all but three sources we estimate the dust extinction to be negligible. In two sources (J1130+0058 and J1207+3352) we obtain a dust extinction of the order of $A_V \sim 1$ mag and the highest extinction ($A_V \sim 2$ mag) is observed for J1600+2058. The amount of dust observed in the X-shaped radio quasar J1130+0058 may explain why this source displays a broad $H\alpha$ but only a narrow $H\beta$ emission line.

The general lack of large amounts of dust in the nuclear environments of X-shaped radio galaxies indicates that any galaxy merger must have happened a long time ago. This conclusion is similar to that drawn by authors who studied the host galaxies of X-shaped sources with optical imaging. They find them to be almost perfectly elliptical, without the usual signs of a recent interaction, such as, e.g., tidal tails or extended dust lanes (e.g., Wirth et al. 1982; van Breugel et al. 1983; Capetti et al. 2002; Cheung & Springmann 2007; Saripalli & Subrahmanyan 2009).

5.2.2 Electron Densities and Temperatures

The flux ratio between the lines of the sulphur doublet [S II] $\lambda\lambda 6716, 6731$ is a suitable indicator of electron density (the higher its value, the lower the density) in the interme-

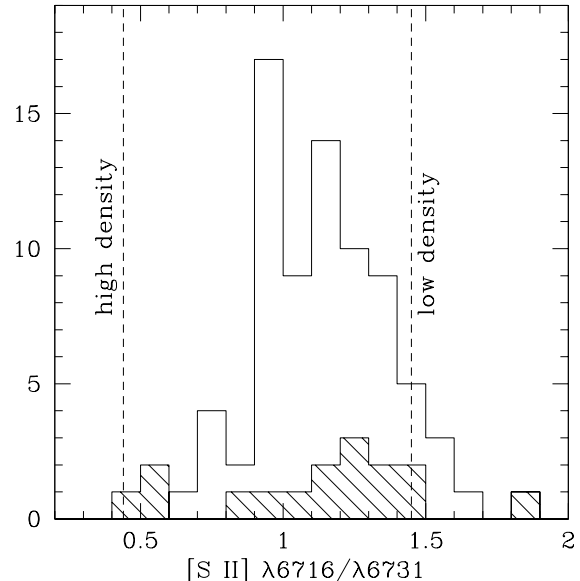


Figure 5. Histogram of the flux ratio between the sulphur lines [S II] $\lambda\lambda 6716, 6731$ for X-shaped sources (shaded) and radio galaxies from the 3CR survey. This ratio is sensitive to the electron density in the intermediate regime of $n_e \approx 10 - 10^5 \text{ cm}^{-3}$, marked by the dashed lines.

mediate regime of $n_e \approx 10 - 10^5 \text{ cm}^{-3}$ (e.g., Peterson 1997). We detect the two sulphur lines in 16/28 sources, of which equal numbers are classified as weak-lined and strong-lined AGN. In Fig. 5 we compare their [S II] line ratios with those observed for a sample of 76 'normal' radio galaxies from the 3CR survey (Buttiglione et al. 2009). We note that we have excluded from the 3CR comparison sample sources in common with our sample. Fig. 5 shows that X-shaped sources reach both higher and lower electron densities than is typical of radio galaxies, however, according to a Kolmogorov-Smirnov (KS) test the distributions of the two groups are not significantly different ($P < 95\%$).

The flux ratio between the sum of the oxygen doublet [O III] $\lambda\lambda 4959, 5007$ and the oxygen line [O III] $\lambda 4363$ is a suitable indicator of electron temperature (the higher its value, the lower the temperature). We detect the [O III] $\lambda 4363$ line in 19/28 sources. These sources are all classified as strong-lined radio-loud AGN. In Fig. 6 (top panel) we have plotted the distribution of the observed oxygen ratios, which suggests that the large majority of X-shaped sources have relatively high electron temperatures. Using a theoretical relation calculated following Osterbrock & Ferland (2006) and assuming an electron density of $n_e = 10^4 \text{ cm}^{-3}$ (Fig. 6, lower panel), we estimate for 13/19 sources temperatures well in excess of the typical value of $T \sim 15,000$ K, with eight sources even exceeding the upper boundary of $T \sim 25,000$ K usually derived for AGN narrow emission line regions (e.g., Peterson 1997).

We note that the [O III] $\lambda 4363$ emission line is usually difficult to measure in AGN, since it is often weak and can blend with $H\gamma$. However, in particular in the aforementioned 13 sources, we observe this line to be relatively strong with typically a rest-frame equivalent width of $W_\lambda \sim 5 \text{ \AA}$ for a signal-to-noise ratio in the continuum of $S/N \sim 20$. Fur-

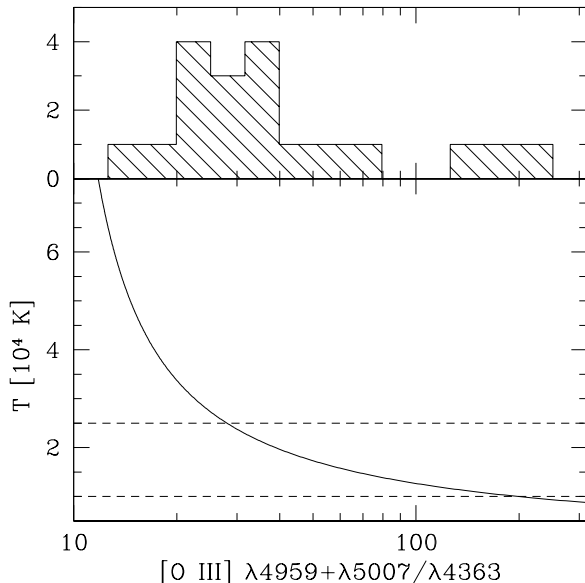


Figure 6. Top panel: Histogram of the flux ratio between the oxygen doublet [O III] $\lambda\lambda 4959, 5007$ and [O III] $\lambda 4363$ for X-shaped sources. Bottom panel: Theoretical relation between this ratio and the electron temperature calculated following Osterbrock & Ferland (2006) and assuming an electron density of $n_e = 10^4 \text{ cm}^{-3}$. The dashed lines mark the temperature range usually derived for AGN narrow emission line regions.

thermore, the resolution of the majority of the spectra is sufficient to reliably separate it from $H\gamma$.

Our results hint at increased pressures being present in the nuclear environments of X-shaped radio galaxies, mainly caused by elevated temperatures. Such enhanced pressures are necessary in the backflow model of Capetti et al. (2002), which proposed that wings emerge in addition to lobes when the jet is orientated along the major axis of the host galaxy. Then, in such a case, the jet lobe becomes overpressured and radio plasma will eventually escape along the galaxy minor axis. In this respect we note that, contrary to our results, the X-ray studies of Hodges-Kluck et al. (2010) found no significant differences in temperature (or density) between a sample of eight X-shaped sources and a sample of 18 ‘normal’ radio galaxies.

6 THE HOST GALAXY

The spectrum of the host galaxy can also put constraints on models for the origin of the X-shaped radio morphology. In particular, if a recent galaxy merger was the source of a change in jet direction, we expect to see spectral signs of starburst activity, such as strong hydrogen absorption lines that are typical of young stars or enhanced continuum flux at short wavelengths.

In order to investigate the properties of the host galaxy spectra of X-shaped radio sources, we have created a composite. For this purpose we have used only those sources in our sample that had a ‘pure’ host galaxy spectrum, i.e., had no [O II] or [O III] emission lines and a Ca II break value of $C \geq 0.4$ (8 objects). The latter constraint ensured that the

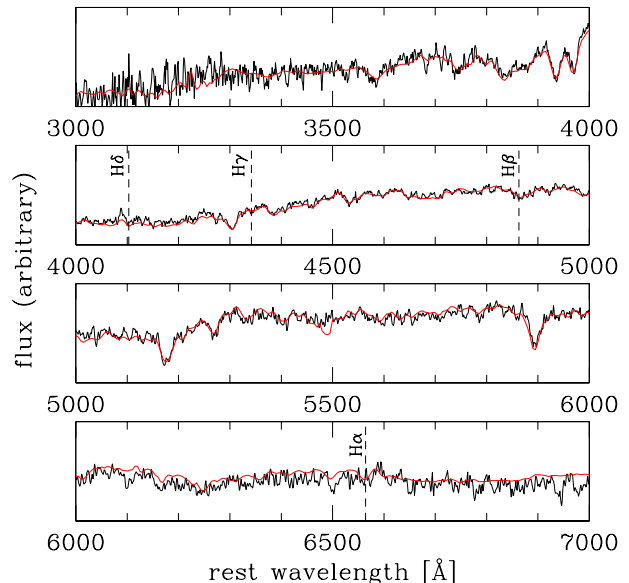


Figure 7. Composite host galaxy spectrum for X-shaped radio sources without [O II] or [O III] emission lines and Ca II break values of $C \geq 0.4$ (black solid line), compared to the elliptical galaxy template of Mannucci et al. (2001) (red solid line). The dashed lines mark the locations of the strongest Balmer hydrogen absorption lines.

blue part of the spectrum was not enhanced by the jet at any perceptible level (see Fig. 1 in Landt et al. 2002), which could otherwise be wrongly interpreted as a sign of enhanced star formation.

Fig. 7 shows the resulting composite host galaxy spectrum (black solid line), compared to the elliptical galaxy template of Mannucci et al. (2001) (red solid line). There are no pronounced differences present between the two spectra, and in particular none of the Balmer hydrogen absorption lines $H\alpha$, $H\beta$, $H\gamma$ or $H\delta$ appear unusually strong.

This result indicates, similar to that of Section 5.2.1, that any galaxy merger must have happened a considerable time ago. Since the starburst should be observable for at least a few million years after its initiation, which is of the order of the electron radiative lifetimes, this then means that the secondary wings are unlikely to be plasma from the old jets and are rather backflow from the currently active lobes.

7 SUMMARY AND CONCLUSIONS

We have analysed the optical spectral properties of a large sample (53 objects) of X-shaped radio sources. The large majority of our sample are radio galaxies, but seven sources are radio quasars (i.e., have broad emission lines). We have considered the general relation between radio and emission line power, searched for signs of recent merger activity and looked for probes of the nuclear environment. Our main results can be summarized as follows:

- (i) The X-shaped radio population contains roughly equal numbers of sources with a weak and a strong emission line spectrum. Given also that their radio powers mostly straddle the dividing line between FR I and FR II radio

Table 3. Narrow Emission Line Fluxes

Object Name	Observatory	class	H α λ 6563 flux [erg/s/cm ²]	H β λ 4861 flux [erg/s/cm ²]	H γ λ 4340 flux [erg/s/cm ²]	[S II] λ 6716 flux [erg/s/cm ²]	[S II] λ 6731 flux [erg/s/cm ²]	[O III] λ 4363 flux [erg/s/cm ²]	[O III] flux ratio (10)
(1)	(2)	(3)	(4)	(5)	(6)	(7)	(8)	(9)	(10)
J0049+0059	SDSS 2.5 m	WL	7.68E-17	–	–	8.14E-17	6.58E-17	–	–
J0113+0106	Shane 3 m	SL	?	1.47E-15	7.05E-16	?	?	1.96E-16	133
J0115-0000	Shane 3 m	SL	?	2.18E-16	1.40E-16	?	?	4.56E-17	34
J0220-0156	MMT 6.5 m	SL	3.75E-15	1.15E-15	5.91E-16	6.03E-16	6.35E-16	5.63E-16	16
J0245+1047	MMT 4.5 m	SL	4.60E-15	–	6.90E-16	–	–	1.60E-15	17
J0516+2458	MMT 6.5 m	SL	6.07E-15	2.16E-15	1.02E-15	3.37E-15	3.28E-15	–	–
J0702+5002	HJST 2.7 m	WL	1.53E-15	3.66E-16	3.10E-16	7.11E-16	1.22E-15	–	–
J0805+2409	SDSS 2.5 m	SL	9.23E-15	2.40E-15	1.55E-15	3.53E-15	2.69E-15	1.11E-15	29
J0831+3219	SDSS 2.5 m	WL	1.00E-15	–	–	1.09E-15	7.36E-16	–	–
J0941+3944	SDSS 2.5 m	SL	3.81E-15	9.04E-16	9.23E-16	1.02E-15	8.38E-16	6.02E-16	26
J1015+5944	SDSS 2.5 m	SL	?	2.54E-16	1.72E-16	?	?	1.27E-16	21
J1020+4831	SDSS 2.5 m	WL	1.29E-15	–	–	9.44E-16	7.84E-16	–	–
J1101+1640	MMT 6.5 m	WL	9.06E-16	–	–	9.86E-16	7.52E-16	–	–
J1130+0058	SDSS 2.5 m	SL	5.66E-15	1.51E-15	6.77E-16	1.13E-15	9.70E-16	3.08E-16	65
J1140+1057	SDSS 2.5 m	WL	3.20E-16	–	–	2.32E-16	4.36E-16	–	–
J1206+3812	SDSS 2.5 m	SL	?	1.79E-16	9.98E-17	?	?	8.19E-17	35
J1207+3352	SDSS 2.5 m	SL	8.16E-15	1.90E-15	9.51E-16	2.63E-15	2.24E-15	6.38E-16	39
J1218+1955	MMT 6.5 m	SL	?	1.25E-16	5.98E-17	?	?	7.57E-17	22
J1310+5458	HET 9.2 m	SL	6.08E-16	2.11E-16	1.24E-16	–	–	1.19E-16	24
J1327-0203	SDSS 2.5 m	WL	1.34E-16	–	–	2.54E-16	1.41E-16	–	–
J1342+2547	HET 9.2 m	SL	?	6.30E-17	5.90E-17	?	?	1.91E-17	21
J1357+4807	HET 9.2 m	SL	1.41E-15	3.78E-16	2.27E-16	–	–	2.36E-17	169
J1430+5217	SDSS 2.5 m	SL	?	5.22E-16	3.17E-16	?	?	1.37E-16	36
J1600+2058	MMT 6.5 m	SL	1.19E-15	1.53E-16	8.77E-17	6.18E-16	4.22E-16	3.35E-17	50
J1606+0000	ESO 3.6 m	WL	2.08E-16	–	–	8.00E-16	9.63E-16	–	–
J1625+2705	SDSS 2.5 m	SL	?	3.66E-16	1.83E-16	?	?	1.47E-16	27
J1952+0230	ESO 2.2 m	SL	?	5.57E-15	4.43E-15	?	?	2.04E-15	56
J2347+0852	KPNO 2.1 m	SL	2.46E-15	1.11E-15	4.02E-16	2.12E-16	4.74E-16	1.28E-16	247

The columns are: (1) object name; (2) observatory at which the spectrum was obtained; (3) classification; (4) - (9) fluxes of the narrow emission lines as labeled, where ?: line position not covered by spectrum, and – : line position covered by spectrum, but line not detected; and (10) flux ratio [O III] λ 4959 + λ 5007/ λ 4363, calculated assuming the theoretical flux ratio [O III] λ 5007/ λ 4959 \approx 3.

galaxies, we show that this kind of sources are the archetypal transition population. We observe a clear transition point in both narrow emission line and radio power at $L_{\text{NLR}} \sim 10^{35}$ W and $L_r \sim 10^{25.6}$ W Hz⁻¹, respectively.

(ii) We have searched for signs of a recent galaxy merger, such as, unusually broad emission lines that would indicate a (large-separation) binary black hole, dusty nuclear environments as probed by the narrow emission lines, and signs of enhanced star formation in the host galaxy. All three approaches gave negative results, suggesting that any merger must have occurred a considerable time ago (longer than the electron radiative lifetimes), thus making it improbable that the pair of wings are relic radio emission.

(iii) We have probed the electron densities and temperatures in the nuclear environments of X-shaped radio sources using narrow emission line diagnostics. We find that the majority of sources have relatively high temperatures ($T \gtrsim 15,000$ K). This supports the scenario where overpressured environments rather than recent mergers seem to be the cause for the X-shape radio morphology.

ACKNOWLEDGMENTS

We thank Mark Lacy, Philip Best and Clive Tadhunter for providing spectra in electronic format. We are indebted to Kirk Korista for providing the results from the Cloudy photoionization code calculations. An anonymous reviewer provided useful suggestions that helped us to improve the paper.

REFERENCES

- Aars C. E., Hough D. H., Yu L. H., Linick J. P., Beyer P. J., Vermeulen R. C., Readhead A. C. S., 2005, *AJ*, 130, 23
- Abazajian K. N., Adelman-McCarthy J. K., Agüeros M. A., Allam S. S., Allende Prieto C., An D., Anderson K. S. J., Anderson S. F., et al., 2009, *ApJS*, 182, 543
- Becker R. H., White R. L., Helfand D. J., 1995, *ApJ*, 450, 559
- Best P. N., 2009, *Astronomische Nachrichten*, 330, 184
- Best P. N., Röttgering H. J. A., Lehnert M. D., 1999, *MNRAS*, 310, 223
- Black A. R. S., Baum S. A., Leahy J. P., Perley R. A., Riley J. M., Scheuer P. A. G., 1992, *MNRAS*, 256, 186

- Boroson T. A., Lauer T. R., 2009, *Nature*, 458, 53
- Brotherton M. S., 1996, *ApJS*, 102, 1
- Buttiglione S., Capetti A., Celotti A., Axon D. J., Chibera M., Macchetto F. D., Sparks W. B., 2009, *A&A*, 495, 1033
- Capetti A., Zamfir S., Rossi P., Bodo G., Zanni C., Masaglia S., 2002, *A&A*, 394, 39
- Cardelli J. A., Clayton G. C., Mathis J. S., 1989, *ApJ*, 345, 245
- Cheung C. C., 2007, *AJ*, 133, 2097
- Cheung C. C., Healey S. E., Landt H., Verdoes Kleijn G., Jordán A., 2009, *ApJS*, 181, 548
- Cheung C. C., Springmann A., 2007, in L. C. Ho & J.-W. Wang ed., *The Central Engine of Active Galactic Nuclei* Vol. 373 of *Astronomical Society of the Pacific Conference Series*, FIRST “Winged” and “X”-shaped Radio Source Candidates. p. 259
- Corbin M. R., 1997, *ApJS*, 113, 245
- De Robertis M., 1985, *ApJ*, 289, 67
- Dennett-Thorpe J., Scheuer P. A. G., Laing R. A., Bridle A. H., Pooley G. G., Reich W., 2002, *MNRAS*, 330, 609
- Dickey J. M., Lockman F. J., 1990, *ARA&A*, 28, 215
- Ekers R. D., Fanti R., Lari C., Parma P., 1978, *Nature*, 276, 588
- Ferland G. J., Korista K. T., Verner D. A., Ferguson J. W., Kingdon J. B., Verner E. M., 1998, *PASP*, 110, 761
- Gaskell C. M., 1996, *ApJ*, 464, L107
- Gopal-Krishna Biermann P. L., Wiita P. J., 2003, *ApJ*, 594, L103
- Hodges-Kluck E. J., Reynolds C. S., Cheung C. C., Miller M. C., 2010, *ApJ*, 710, 1205
- Kraft R. P., Hardcastle M. J., Worrall D. M., Murray S. S., 2005, *ApJ*, 622, 149
- Lacy M., 2000, *ApJ*, 536, L1
- Laing R. A., Jenkins C. R., Wall J. V., Unger S. W., 1994, in Bicknell G. V., Dopita M. A., Quinn P. J., eds, *The First Stromlo Symposium: The Physics of Active Galaxies Spectrophotometry of a complete sample of 3CR radio sources: Implications for unified models*. A.S.P., San Francisco, p. 201
- Lal D. V., Rao A. P., 2007, *MNRAS*, 374, 1085
- Landt H., Bignall H. E., 2008, *MNRAS*, 391, 967
- Landt H., Padovani P., Giommi P., 2002, *MNRAS*, 336, 945
- Landt H., Padovani P., Perlman E. S., Giommi P., 2004, *MNRAS*, 351, 83
- Leahy J. P., Parma P., 1992, in Roland J., Sol H., Pelletier G., eds, *Extragalactic Radio Sources. From Beams to Jets Multiple outbursts in radio galaxies*. Cambridge University Press, p. 307
- Leahy J. P., Williams A. G., 1984, *MNRAS*, 210, 929
- Ledlow M. J., Owen F. N., 1996, *AJ*, 112, 9
- Mannucci F., Basile F., Poggianti B. M., Cimatti A., Daddi E., Pozzetti L., Vanzi L., 2001, *MNRAS*, 326, 745
- Marziani P., Sulentic J. W., Dultzin-Hacyan D., Čalvani M., Moles M., 1996, *ApJS*, 104, 37
- Merritt D., Ekers R. D., 2002, *Science*, 297, 1310
- Miller B. P., Brandt W. N., 2009, *ApJ*, 695, 755
- Murgia M., Parma P., de Ruiter H. R., Bondi M., Ekers R. D., Fanti R., Fomalont E. B., 2001, *A&A*, 380, 102
- Osterbrock D. E., Ferland G. J., 2006, *Astrophysics of Gaseous Nebulae and Active Galactic Nuclei*. University Science Books
- Perlman E. S., Padovani P., Giommi P., Sambruna R., Jones L. R., Tzioumis A., Reynolds J., 1998, *AJ*, 115, 1253
- Peterson B. M., 1997, *An Introduction to Active Galactic Nuclei*. Cambridge University Press
- Peterson B. M., Korista K. T., Cota S. A., 1987, *ApJ*, 312, L1
- Rawlings S., Saunders R., 1991, *Nature*, 349, 138
- Rottmann H., 2001, PhD thesis, Rheinische Friedrich-Wilhelms-Universität Bonn
- Saripalli L., Subrahmanyam R., 2009, *ApJ*, 695, 156
- Shen Y., Loeb A., 2009, *ArXiv e-prints*
- Tadhunter C. N., Morganti R., di Serego-Alighieri S., Fosbury R. A. E., Danziger I. J., 1993, *MNRAS*, 263, 999
- Tadhunter C. N., Morganti R., Robinson A., Dickson R., Villar-Martin M., Fosbury R. A. E., 1998, *MNRAS*, 298, 1035
- Ulrich M., Roennback J., 1996, *A&A*, 313, 750
- van Breugel W., Balick B., Heckman T., Miley G., Helfand D., 1983, *AJ*, 88, 40
- Wang T., Zhou H., Dong X., 2003, *AJ*, 126, 113
- Wirth A., Smarr L., Gallagher J. S., 1982, *AJ*, 87, 602
- Worrall D. M., Birkinshaw M., Cameron R. A., 1995, *ApJ*, 449, 93
- Zhang X., Dultzin-Hacyan D., Wang T., 2007, *MNRAS*, 377, 1215

APPENDIX A: SDSS SPECTRA

This paper has been typeset from a $\text{\TeX}/\text{\LaTeX}$ file prepared by the author.

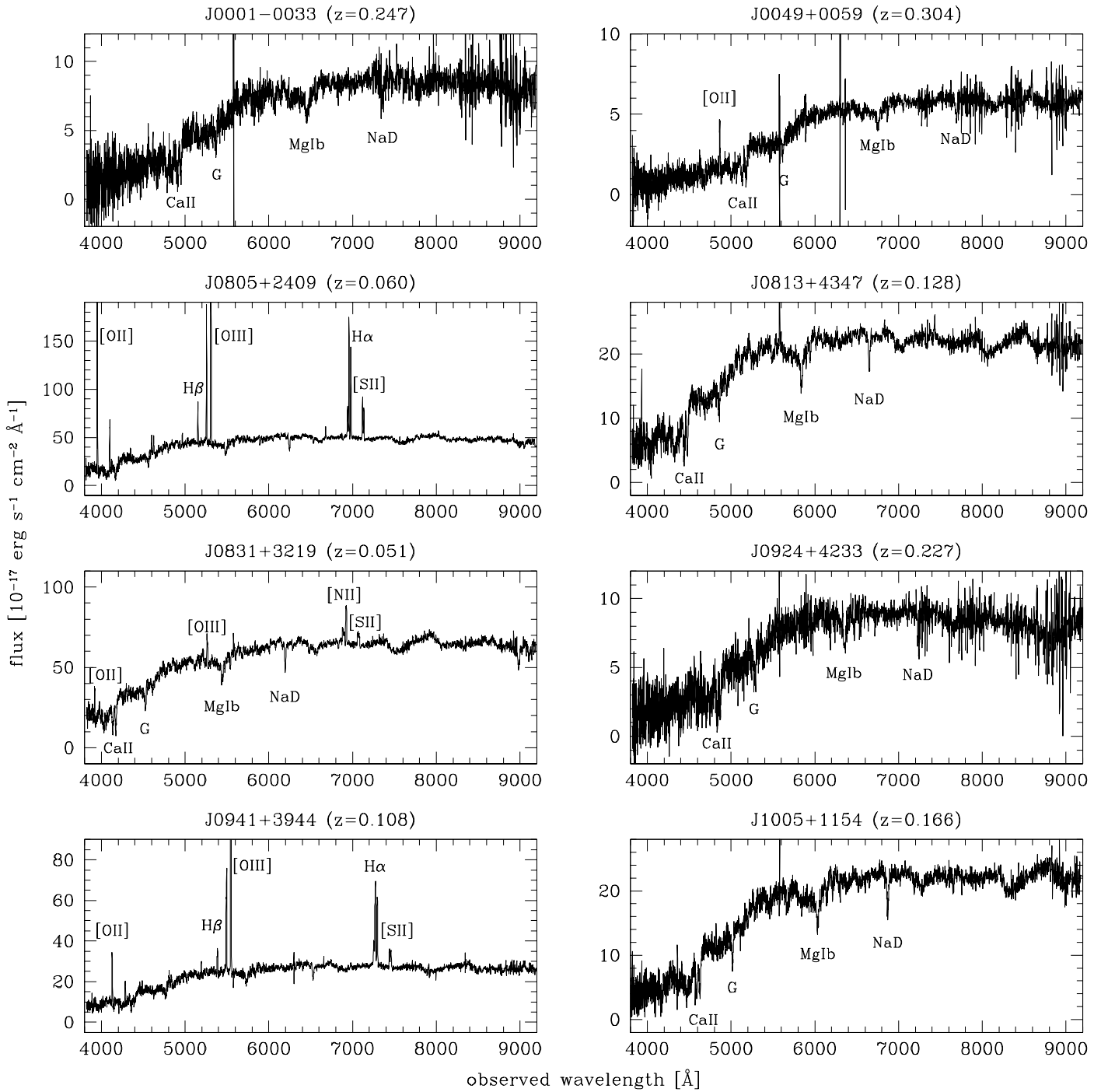


Figure A1. Observed Sloan Digital Sky Survey (SDSS) spectra (corrected for Galactic extinction) of X-shaped radio sources.

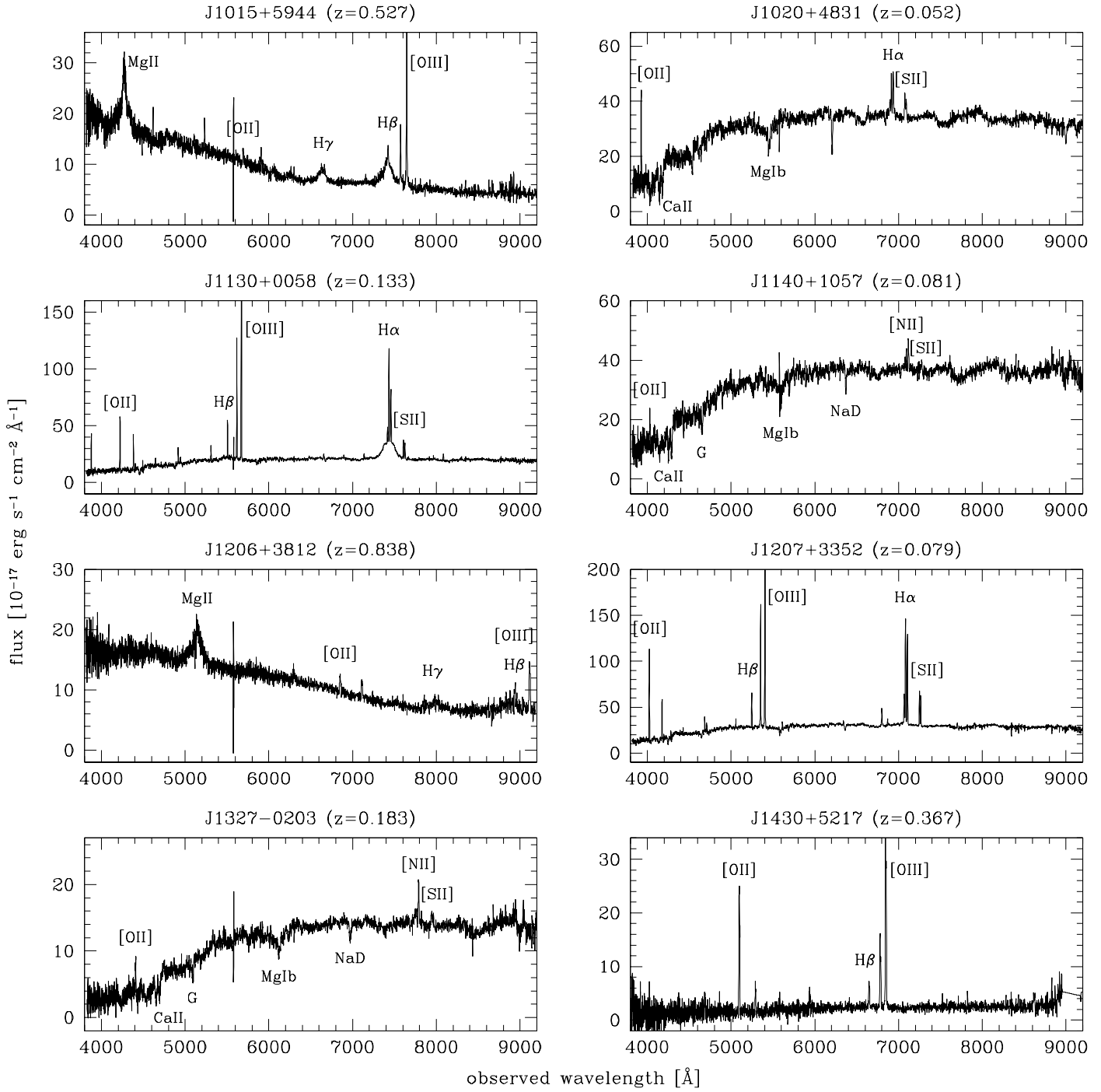


Figure A1 – continued

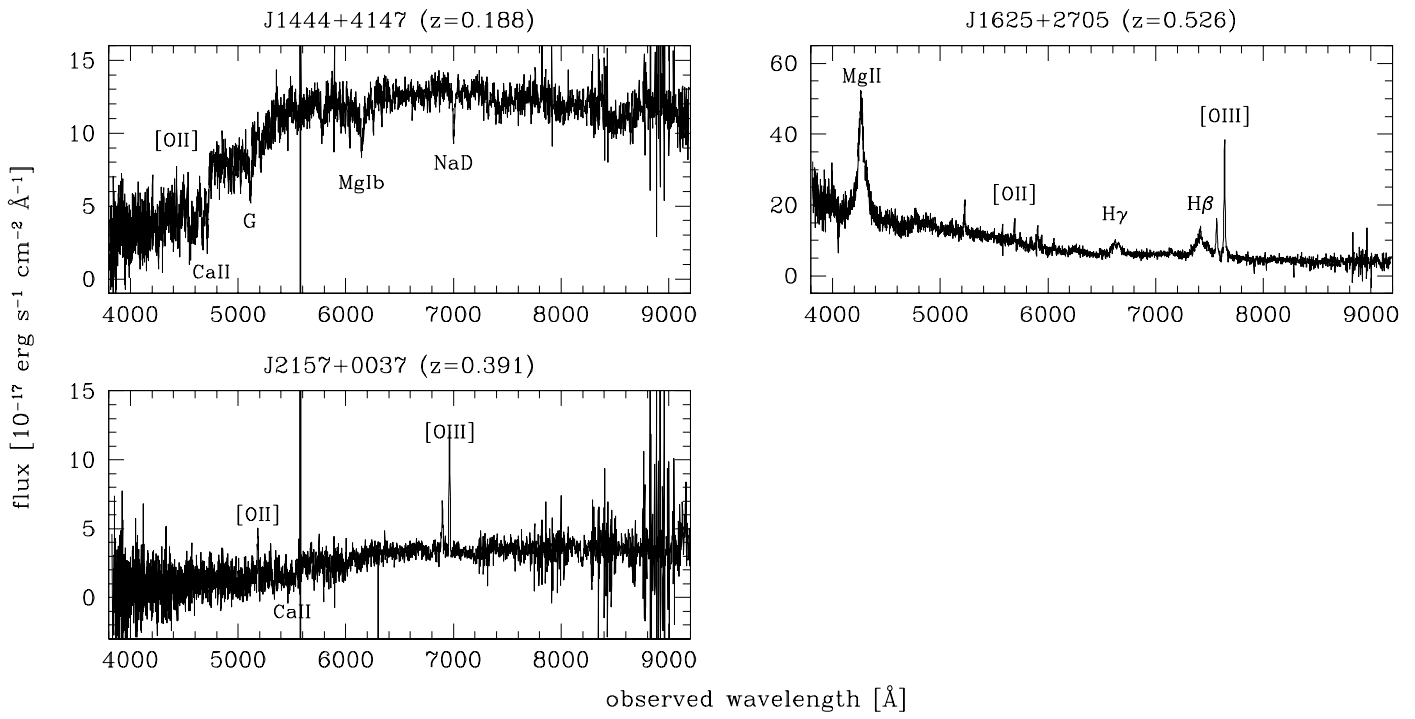


Figure A1 – *continued*